

The response of a tensioned flexible sheet immersed in parallel flow

Michael T. Morris-Thomas[†] and Sverre Steen

Department of Marine Technology, Norwegian University of Science and Technology,
Otto Niensens vei 10, Trondheim, NO-7491, Norway. [†]E-mail: michaelmorristhomas@gmail.com

Abstract

This paper explores the fluid-elastic response of a cantilevered flexible sheet in the presence of uniform airflow. The leading edge of the sheet is clamped, while at the trailing edge, in-plane tension is applied to provide additional rigidity to the sheet's small but finite bending stiffness. We outline a series of experiments performed in a wind tunnel with the purpose of examining fluid-elastic instabilities. In particular, we examine the role of in-plane tension induced rigidity and how it influences static divergence and convected wave instabilities. The flow is characterised by Reynolds numbers of order 10^5 - 10^6 and we specifically examine a sheet with an aspect ratio of $L/l = 1.33$. A unique aspect of this present work, is the direct measurement of the sheet's three-dimensional displacement through an optical tracking method with a grid of passive markers placed on the sheet surface. We show the evolution of the sheet surface from stability, through to divergence, and then finally into flutter. The frequency composition of the flutter event shows higher harmonic components that suggest significant nonlinearities. Tension induced rigidity plays a crucial role in the response of the sheet to the fluid in both postponing and suppressing instabilities.

1 Introduction

The response of a flexible surface immersed in a moving fluid is a ubiquitous fluid-structure interaction problem. It can be observed in everyday life from the motion of a leaf fluttering in a mild breeze, to the locomotion of insects, birds and waterborne animals, to more abstract applications like snoring and marine vehicles. Despite this ubiquity, much is still to be understood because the inherent fluid-elastic coupling of the problem poses certain difficulties in determining fluid-elastic stability characteristics. Consequently, this limits our understanding of a flexible surface's response under large displacements, the scaling of its fluid dynamic drag, three-dimensional effects, and the role of both shear and oscillatory boundary layers. In this present work we experimentally examine the behaviour of a flexible sheet both before and after stability is lost with particular emphasis on static divergence, convected wave instability modes, and the influence of tension applied at the trailing edge of the sheet on these instabilities.

A flexible sheet immersed in a flowing fluid can experience instability when the incident fluid velocity breaches some critical value [1]. The nature of this instability depends upon competition between the sheet's inertia, fluid momentum, and the restorative influences of its flexural rigidity and axial or lateral tension — which can be supplied by either the boundary layer or by external means. At the onset of instability, which can be caused through any significant perturbation of the system, the manner in which these characteristics of the system interact can result in either a

convected wave type of instability [2, 3, 4] or static divergence [5]. We shall denote the velocity at which these occur U_s and U_c for static divergence and convected waves respectively. A convected wave type of instability is characterised by dispersive waves that originate at the leading edge of the sheet and propagate towards the trailing edge. This type of instability is often referred to as flutter where U_c is thought of as the critical velocity for a global instability. On the other hand, in the event of divergence, the sheet typically adopts an alternative mean position in response to the flow that can be one of infinitely many possible mode shapes. Typically, if divergence is to be realised then $U_s < U_c$. In both instability regimes, this self-excited response can adversely affect the sheets hydrodynamic performance, fluid dynamic drag, and can lead to more chaotic behaviour — see Connell and Yue’s [4] Figure 23 for instance.

To simplify a description and aid in our understanding of the fluid-elastic coupling of the problem, we can divide the nature of the surrounding fluid flow into two regimes based on the sheet aspect ratio $\mathcal{A} = L/l$ where L and l denote the sheet length and width respectively. For $\mathcal{A} \gg 1$, we essentially have a long slender sheet and the flow about it can be considered approximately two-dimensional in the cross-flow direction. Here, flow separation at the trailing edge is of little consequence compared to boundary layer induced tension and fluid added mass effects. Such a characterisation would encompass the performance of long slender bodies of more general cross-section [6] and in particular ribbons and streamers [7, 8, 9, 10].

On the other hand, when $\mathcal{A} = \mathcal{O}(1)$, the characteristics of the flow are far more complicated due to the three-dimensionality of the sheet and the importance of flow separation and shear layers in the form of an unsteady wake and downwash over the cross-flow direction. In a strictly two-dimensional setting, the effect of an unsteady wake on a sheet of infinite width has been considered both theoretically [11, 2, 12] and experimentally in the illuminating soap film experiments of Zang and associates in a post-critical regime [13]. However, in the regime $\mathcal{A} = \mathcal{O}(1)$, the coupling of unsteadiness with the effects of three-dimensionality has only recently been approached numerically [3] with some success at determining the critical flow velocity for a flexible sheet and its qualitative behaviour after stability is lost.

For sheets comprising small flexural rigidity, the majority of previous experimental studies concern the regime $\mathcal{A} \gg 1$. Here, the sheet is often mounted vertically [14, 7, 10] allowing gravity to provide additional restorative restraint to flexure. On the other hand, it is possible to mount a flexible sheet horizontally in flow with axial tension [15], lateral tension [16] or a combination of both [17]. This approach is advantageous if one wishes to quantify the effect of tension induced rigidity on instability. In a recent experimental campaign, Morris-Thomas and Steen [17] considered the regime $\mathcal{A} = \mathcal{O}(1)$ with trailing edge tension providing additional rigidity both axially and laterally to a flexible sheet. The authors demonstrated that axial tension can temporarily postpone fluid-elastic instability, leading to a reduction in fluid dynamic drag, and consequently suppressing the expected rise in drag once stability is lost. However, although the relationship between stability and drag were examined, no direct measurement of the displacement of the sheet surface was performed. At present we lack quantitative information concerning the three-dimensional performance of a flexible sheet, how in-plane tension affects the growth and nature of fluid-elastic instabilities, and the consequences of these to the fluid

dynamic drag. We are not aware of any experimental studies that attempt a direct measure of the three-dimensional displacement of a flexible sheet in flow. We intend to address this situation here and present some results from our recent experimental study.

We investigate the fluid-elastic response of a cantilevered sheet of low flexural rigidity B and mass per unit area m immersed in uniform airflow defined by velocity U . The sheet is mounted horizontally in the flow and tension is supplied at the trailing edge. We describe a set of experiments that were performed on the configuration in a wind tunnel. A test matrix comprising Reynolds numbers of order 10^5 - 10^6 , sheet aspect ratios $\mathcal{A} = 1.33$ - 2.0 , and a variation in trailing edge tension was considered. The displacement of the sheet surface was monitored via an optical tracking system whereby a linear grid of approximately 100 retro-reflective markers was placed on the sheet surface. The utility of this approach allows us to study the evolution of the sheet surface from a stable into an unstable state without intruding on the fluid flow. In this paper, we examine the trajectories provided by these passive markers for one particular sheet $\mathcal{A} = 1.33$. This provides a unique view into static divergence and convected wave type instabilities acting over the surface of a sheet. Furthermore, we examine these instabilities in the presence of a parametric variation of tension induced rigidity acting on the trailing edge of the sheet. The paper is organised as follows: a description of the experimental campaign undertaken is given in §2; a discussion of the experimental results in terms of flutter and divergence is provided §3; and finally, conclusions and suggestions for future work are outlined in §4.

2 Experimental Campaign

Experiments were conducted in the low speed wind tunnel of the Aerodynamics Laboratory at the Norwegian University of Science and Technology. The tunnel comprises an available test section of $2.7\text{m} \times 1.83\text{m}$ and allows fluid velocities up to 30ms^{-1} with a turbulence intensity of less than 5%. The experimental set-up and testing matrix is in some respects an extension of that described by Morris-Thomas and Steen [17]. However, while this expanded experimental campaign employs a smaller test matrix, it encompasses direct measurements of the sheet displacement under flow.

A transparent Polyethylene sheet of thickness $h = 0.15\text{mm}$ and width $l = 75\text{cm}$ was mounted horizontally along the centre-line of the test section with a clamped leading edge and free trailing edge. The set-up is illustrated in Figure 1. The bottom of the sheet was located 54cm above the base of the wind tunnel avoiding the developing turbulent boundary layer along the wind tunnel floor and walls. The pertinent characteristic of the sheet include a small flexure rigidity $B = 59.7 \times 10^{-6}\text{Nm}^2\text{m}^{-1}$ to allow the observation of flexural waves and a small mass per unit area $m = 0.14\text{kgm}^{-2}$. At the trailing edge of the sheet, tension was applied via nylon strings attached to the top and bottom vertices of the sheet (cf. Figure 1). Each string left the trailing edge at a known angle θ and travelled through a pulley system that directed it underneath the wind tunnel where it was attached to a known weight providing a combined pre-tension T .

A typical test run involved gradually increasing the fluid velocity in the wind tunnel over increments of approximately 0.2 - 0.5ms^{-1} until instability of the flexible sheet was observed.

Testing then continued up to fluid velocities of approximately $U_c + 2\text{ms}^{-1}$. The testing matrix adopted here is summarised in Table 1 where we note a parametric variation of the sheet’s aspect ratio $\mathcal{A} = L/l$, the magnitude of combined tension and the angle at which it was applied to the trailing edge. The measurable quantities of interest to us are the fluid dynamic drag experienced by the sheet, the mean and dynamic tension at the trailing edge and the displacement of the sheet surface.

2.1 Apparatus

In order to acquire the displacement of the sheet surface we employed optical tracking. The advantage of such a system is that it allows a non-intrusive approach to measuring the displacement of the sheet surface without disrupting the fluid flow. The flexible sheet was fitted with a grid of retro-reflective markers each comprising a 4mm diameter. These passive markers were spaced at 50mm intervals in the flow direction and 180mm in the cross-flow direction. This provided a grid of 100 markers with five columns for a sheet length of 1m. These markers can be observed in Figure 1. The displacement or trajectories of these markers in space was captured with two ProReflex motion capture cameras. These cameras were mounted in a vertical alignment outside the wind tunnel approximately 2m from the centre-line of the sheet surface. Vertical alignment, such that the top and bottom cameras were positioned above and below the top and bottom edges of the sheet respectively, was chosen to avoid refraction errors introduced by the perspex panels of the wind tunnel and sheet surface itself. The origin of the (x, y, z) co-ordinate system was located at the bottom of the leading edge of the sheet. The positive x -axis is directed down the sheet length and the positive z -axis defines the location of the leading edge. Dynamic calibration of the optical tracking system was performed approximately every 4 hours of testing.

In addition to the sheet displacement, we also recorded the external tension applied to the trailing edge and the fluid dynamic drag experienced by the sheet. For the tension, a ring type strain gauge was located on each nylon string line immediately behind the trailing edge. The fluid dynamic drag was measured by using a three component force balance situated under the centre of the test section. The leading edge of the sheet was attached via nylon tape to a 1.43m long vertical pole comprising an elliptical cross-section ($a = 4\text{cm}$, $b = 2\text{cm}$). This pole extended underneath the wind tunnel and was attached to the force balance allowing a direct measure of the fluid dynamic drag. Previous testing utilising this pole [17] showed that its drag coefficient is $C_D = 0.59$ and therefore, its contribution to the overall drag, although minimal, can be subtracted from the in-line force measurements at the force balance. In doing so, and after further subtracting the axial tension, provides us with a measure of the drag experience by the sheet.

The incident flow velocity was measured with a Pitot-static tube located 1m upstream from the leading edge position of the sheet. The fluid properties that we adopt for the analysis are based on a measured air temperature of 20.3°C implying $\rho = 1.205\text{kgm}^{-3}$ and $\nu = 0.150\text{cm}^2\text{s}^{-1}$. Measurements from the Pitot-static tube, force balance and strain gauges were acquired through

a HBM instrumentation amplifier with a wireless connection to a notebook computer running Catman data acquisition software. The measurements from all sensors were digitised at 200Hz and pre-processed through a fifth-order low-pass Butterworth filter with a cut-off frequency of 40Hz. The dominant frequencies of the system, and associated harmonics of interest to us, were all less than approximately 25Hz.

2.2 Post-processing

The digitized images were processed with Qualisys¹ motion tracking software to extract the trajectory $M_n(x_i, y_i, z_i, t_i)$ of each marker n in the global co-ordinate system over time $t = i\Delta t$ where i is an integer. In selecting Δt , the channel capacity of the motion capture cameras forced us to compromise frame rate to allow a suitable amount of passive markers for the sheet. Consequently, choosing an upper bound of $N = 100$ markers provided us with a maximum frame rate of $f = 60Hz$. Furthermore, the available buffer of the cameras meant that we could safely record for time windows of length $T_L = 58s$ before overflow resulted in a loss of markers and hence trajectories. This time window is further shortened should rouge markers be detected by the cameras. To avoid such complications we chose a frame rate of $f = 50Hz$ and operated over time windows of $T_L = 50s$.

With windowing taken into account, each element from the test matrix resulted in approximately 10-17 data sets of constant flow velocity comprising trajectories for around 90-100 markers. The trajectory data was then exported into a standard ASCII format for post-processing in MATLAB. Post-processing revealed several rouge markers introduced through artificial light sources caused by reflections through the perspex wind tunnel walls and the sheet surface. The positions of which were subsequently identified and these markers removed from each data set.

3 Results and Discussion

Typical passive marker positions on the surface of the flexible sheet are shown in Figure 2 for $U = 2.37ms^{-1}$ with a combined tension of $T = 7.95N$ applied at 45° to the trailing edge. The flow direction is from $x = -\infty$ — this is implied for all results presented hereafter. The surface of the sheet appears in the (x, z) so that $x/L = 0$ and $x/L = 1$ correspond to the leading and trailing edges respectively. This particular case illustrates a perfectly stable sheet. When instability results we expect displacements of each marker to occur across the sheet in the (y, z) plane.

In contrast, we now show marker trajectories along the centre-line of the same sheet after stability is lost to flutter. Figure 3 illustrates the trajectories in time for four such markers in the (y, z) plane along the sheet's centre-line at the horizontal positions $x \approx 0.05, 0.35, 0.70$ and 0.95 . We notice that the displacement of the markers in the vertical direction is actually quite small and $\mathcal{O}(1)mm$. The majority of the motion occurs along the y -axis and, as such, the path of the trajectories in the centre of the sheet are mildly elliptical with a large major axis.

¹see <http://www.qualisys.com> for further details regarding the motion capture system and software.

However, at the extremities of the sheet, the clamped boundary condition at the leading edge and the applied tension at the trailing edge, leads to a more restrained horizontal motion. One problem with mounting a sheet horizontally so that its leading edge is vertical is the possibility of introducing asymmetry along the sheet surface. This is caused through the weight of the sheet and we expect this to be more prevalent under small magnitudes of applied tension. Figure 3 actually shows the result of this where one can see the mean vertical position of the markers decreasing as we progress further along the sheet towards the trailing edge.

3.1 Flutter instabilities

A good example of the frequency composition of a flexible sheet once stability is lost to a convected wave instability is illustrated in Figure 4. In this example we focus on a sheet of length $L = 1\text{m}$ in an incident flow velocity of 2.42ms^{-1} with a very moderate combined tension of 2.06N . Here, we have chosen to concentrate on the centre-line of the sheet $z = 0.375$ where values of $x = 0$ and 1 denote the leading and trailing edges respectively. The f axis corresponds to the frequency content of the horizontal displacement of the sheet measured in Hz. In frequency space, this is represented as $\hat{\eta}$ and obtained via a standard Fourier transform algorithm over the signal length for each marker located along the centre-line.

We observe that once stability is lost to flutter, a dominant frequency and associated phase locked harmonic components appear (cf. Figure 4). The appearance of higher harmonic components, the amplitudes of which are certainly not negligible in relation to the first-harmonic, suggest nonlinearities in the system. Presumably, these elastic nonlinearities result from nonlinear sheet curvature which must clearly be important under large displacements incurred through a flutter event. The measurements suggest that the dominant frequency is $f_1 = 0.43\text{Hz}$ with harmonics visible up to $3 \times f_1$. Another interesting feature of the results is that the global maximum of the convected wave amplitude envelop occurs towards the leading edge of the sheet — approximately $x/L = 0.25$. After which, the amplitude monotonically decreases towards a local minimum in the vicinity of the the trailing edge. Although not illustrate here, our results suggest that when the axial tension is increased the position of this maximum amplitude is not significantly affected.

We now draw attention to the dominant or first-harmonic of the instability and examine how this develops over a select range of fluid velocities. To illustrate this, we present Figures 5 and 6. These plots show the spatial distribution of the first-harmonic magnitude of the convected wave instability over the (x, z) plane. It is denoted $|\hat{\eta}_1(x, z)|$. This dominant harmonic was obtained through a direct Fourier transform of the $y(t)$ -component of each marker on the sheet. A band-pass Butterworth filter was then employed to extract the first-harmonic. The positions of the markers in the (x, z) plane were relatively invariant with time compared to the y -component, so the mean positions obtained from the time series' are adopted for the analysis here.

Once stability is lost, the first-harmonic appears quite noticeably over the surface of the sheet. We can infer from Figure 5 that stability is lost to flutter in the vicinity of $2.04 < U_c < 2.49\text{ms}^{-1}$. While under under greater axial tension, this range is translated to $6.77 < U_c < 7.26\text{ms}^{-1}$ (cf.

Figure 6). At the top edge of the sheet, $z = 0.75$, we notice a small flutter event before the dominant convected wave instability covers the entire sheet — see Figure 6 for $U = 6.77\text{ms}^{-1}$. This feature is a localised standing wave and it was more noticeable under higher values of tension at the trailing edge.

Due to the fact that the leading edge of the sheet was mounted vertically, we can expect some asymmetry in the instability under small in-plane tension. This is due to the weight of the sheet and would explain the large amplitudes along the bottom edge $z = 0$ once stability is lost (see Figure 5). The elastic stress distribution, resulting from the applied tension, would presumably be of much lower density in this region which renders it more susceptible to stability loss.

With greater tension applied to the sheet we observe a smaller amplitude of the first-harmonic and much more asymmetry over the sheet surface (cf. Figure 6). Interestingly, under high tension the first-harmonic component is slightly visible before $U = 6.77\text{ms}^{-1}$ as shown in Figure 6, however, its amplitude is extremely small and surrounded by broadband noise.

One aspect of the experiments worth mentioning is the observation of high frequency flutter in the immediate vicinity of the trailing edge. Unfortunately, this was not acquired at sufficient quality by the optical tracking system to yield any quantitative results. However, we observe that this flutter is very localised and does not result in any convective type of instability but rather resembles a localised standing wave. The amplitude of this high frequency event appears largest along the centre-line and does not penetrate any further than approximately $0.05L$ into sheet from the trailing edge.

3.2 Static Divergence

We now examine the mean or zero-harmonic response of the sheet. This should correspond to a static divergent type of instability. For a sheet experiencing a combined tension of 2.06N , the distribution of the mean component over the sheet surface is illustrated in Figure 7. The mean component is denoted $\bar{\eta}$ and the response is shown for a number of fluid velocities ranging from $U = 0.09\text{ms}^{-1}$ up to $U = 3.43\text{ms}^{-1}$ which is beyond the point in which flutter of the sheet was first observed (cf. Figure 5).

The appearance of a static instability is quite visible and the results indicate that it occurs somewhere in the region of $0.1 < U_s < 2\text{ms}^{-1}$. This range is somewhat lower than the flow velocity at which a flutter instability mode first appears (cf. Figure 5). At $U = 0.1\text{ms}^{-1}$ we observe a small mean component in the vicinity of the leading edge along $x = 0$. We suspect this is unrelated to divergence and is merely caused by the weight of the sheet under minimal trailing edge tension. However, it does offer an irregularity or perturbation of the sheet profile that may promote the onset of an instability.

Interestingly, once the sheet loses stability to flutter (cf. Figure 5) we notice a reduction in the mean component across the surface of the sheet. In other words, divergence is being replaced by a convected wave instability and it is quite possible that energy is then transferred to the first-harmonic. In the overlapping region between the two instabilities superposition

would appear to be taking place. However, after the convected wave instability is realised, the static divergent mode is suppressed at $U = 2.5\text{ms}^{-1}$ and it is then almost inconsequential at $U = 3.43\text{ms}^{-1}$ where it has been replaced by flutter (see Figure 7).

It is worth pointing out that under larger magnitudes of applied tension at the trailing edge, no noticeable divergence was observed. Typically, we observe a very small linear increase in the horizontal displacement of the sheet with a maximum at the trailing edge of at most 3cm. An example of this is shown in Figure 8. This small mean component is suppressed by higher fluid velocities and, once U_c is reached, the sheet loses stability to convected waves before any observable static divergence.

4 Conclusions

We have examined the performance of a cantilevered flexible sheet, of aspect ratio $\mathcal{O}(1)$, mounted horizontally in uniform air flow with an external in-plane tension applied to the trailing edge. In particular, an experimental campaign was conducted whereby we investigated the loss of stability of a flexible sheet to both convected waves or flutter and static divergence. The unique aspect of this work was the use of an optical tracking system to measure the displacement of the sheet surface at select marker locations. We studied the trajectories of these markers and performed a harmonic analysis to extract the mode shapes for both divergence and flutter.

Our results have provided a unique insight into the spatial variation and harmonic composition of an unstable sheet in fluid flow. The frequency composition of an unstable sheet shows a dominant frequency component with clearly defined harmonics that suggest the influence of elastic nonlinearities associated with the sheet are important to understanding its performance in a post-critical regime. Moreover, we have shown that a sheet may first lose stability through divergence before being replaced by a convected wave type instability. During the energy transfer, we suspect that there is some superposition between the two instability modes. Under large values of trailing edge tension, with an equal contribution axially and laterally to the sheet, no static divergence of the sheet was observed. On the other hand, a convected wave or flutter type of instability is observed in this region when stability of the sheet is lost. We have also shown that, with increasing trailing edge tension, the mode shape amplitudes of both divergence and flutter are reduced.

Further analysis of these experimental results is required. Of particular interest is the effect of sheet aspect ratio on the behaviour of instability modes and also the influence of lateral tension acting across the sheet. Moreover, we should also like to examine the frequency shift and phasing of the convected wave instability across the sheet as the fluid velocity is increased and the consequences this poses for the fluid dynamic drag. It is the authors' intention to investigate these aspects further.

Acknowledgements

The authors gratefully acknowledge the financial support of the Norwegian Research Council under grant number 169417/530 and Schlumberger. Finally, we thank Rune Toennesen, Schlumberger, for his comments and technical input over the course of this work.

References

- [1] Rayleigh, L., 1879. “On the instability of jets”. *Proc. Lond. Math. Soc.*, **10**(4), pp. 4–13.
- [2] Zhu, L., and Peskin, C. S., 2002. “Simulation of a flapping flexible filament in a flowing soap film by the immersed boundary method”. *Journal of Computational Physics*, **179**, pp. 452–468.
- [3] Tang, D. M., Yamamoto, H., and Dowell, E. H., 2003. “Flutter and limit cycle oscillations of two-dimensional panels in three-dimensional axial flow”. *Journal of Fluids and Structures*, **17**(2), pp. 225–224.
- [4] Connell, B. S. H., and Yue, D. K. P., 2007. “Flapping dynamics of a flag in a uniform stream”. *Journal of Fluid Mechanics*, **581**, pp. 33–67.
- [5] Païdoussis, M. P., 2004. *Fluid-Structure Interactions: Slender Structures and Axial Flow*, Vol. 2. Academic Press, San Diego, California.
- [6] Lighthill, M. J., 1960. “Note on the swimming of slender fish”. *Journal of Fluid Mechanics*, **9**, pp. 305–317.
- [7] Datta, S. K., and Gottenberg, W. G., 1975. “Instability of an elastic strip hanging in an airstream”. *Journal of Applied Mechanics*, **75**, March, pp. 195–198.
- [8] Auman, L. M., and Dahlke, C. W., 2001. “Drag characteristics of ribbons”. In The 16th Aerodynamic Decelerator Systems Technology Conference, AIAA, pp. 131–136.
- [9] Carruthers, A. C., and Filippone, A., 2005. “Aerodynamic drag of streamers and flags”. *Journal of Aircraft*, **42**(4), pp. 976–982.
- [10] Lemaitre, C., Hémon, P., and de Langre, E., 2005. “Instability of a long ribbon hanging in axial air flow”. *Journal of Fluids and Structures*, **20**(7), pp. 913–925.
- [11] Kornecki, A., Dowell, E. H., and O’Brien, J. O., 1976. “On the aeroelastic instability of two-dimensional panels in uniform incompressible flow”. *J Sound Vib.*, **47**(2), pp. 163–178.
- [12] Argentina, M., and Mahadevan, L., 2005. “Fluid-flow-induced flutter of a flag”. *Proceedings of the National Academy of Sciences*, **102**(6), pp. 1829–1834.
- [13] Zhang, J., Childress, S., Libchaber, A., and Shelley, M., 2000. “Flexible filaments in a flowing soap film as a model for one-dimensional flags in a two-dimensional wind”. *Nature*, **408**, pp. 835–839.

- [14] Taneda, S., 1968. “Waving motions of flags”. *Journal of the Physical Society of Japan*, **25**(2), pp. 392–401.
- [15] Coene, R., 1992. “Flutter of slender bodies under axial stress”. *Applied Scientific Research*, **49**(1), pp. 175–187.
- [16] Watanabe, Y., Suzuki, S., Sugihara, M., and Sueoka, Y., 2002. “A experimental study of paper flutter”. *Journal of Fluids and Structures*, **16**(4), pp. 529–542.
- [17] Morris-Thomas, M., and Steen, S., 2009. “Experiments on the stability and drag of a flexible sheet in uniform parallel flow”. *J. Fluids Struct.*, **25**(5), pp. 815–830. [arXiv: 0901.4884v1].

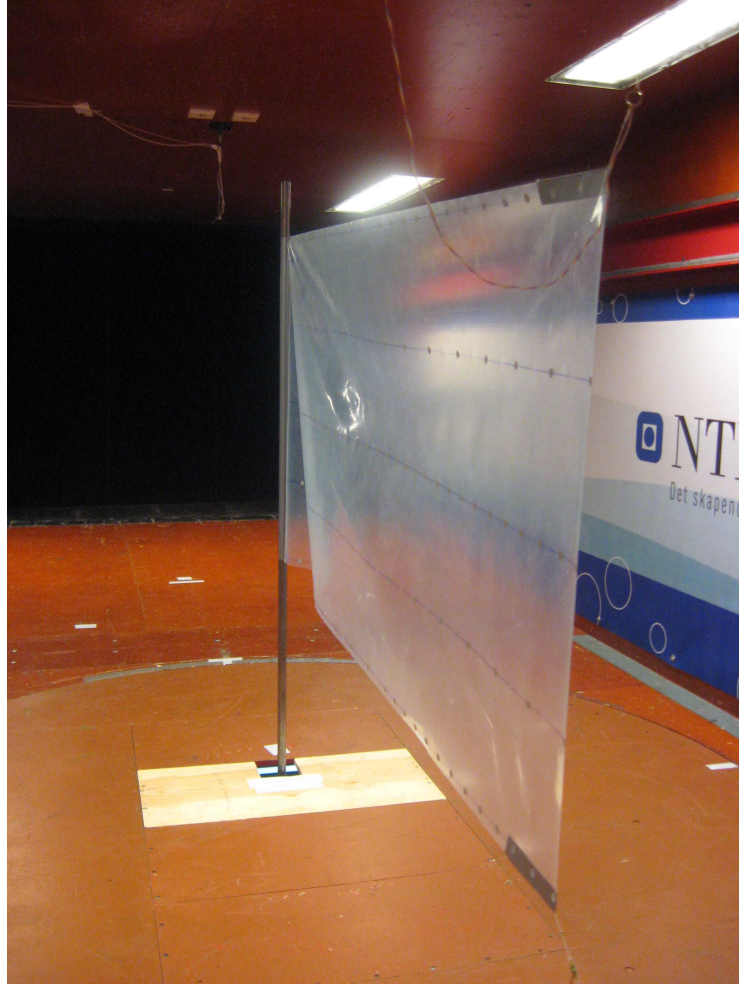


Figure 1: The experimental set-up in the wind tunnel. The retro-reflective markers are pictured in grey over five columns along the sheet surface. Although not pictured, the two ProReflex cameras are located to the left of the image outside the wind tunnel. Two nylon strings are observed at the trailing edge which were used to apply tension.

Table 1: The test matrix employed in the experimental study where \mathcal{A} denotes the aspect ratio, A the sheet surface area, m the mass per unit area, B the flexural rigidity, Re the Reynolds number, T the combined magnitude of tension applied to the trailing edge and θ represents the angle at which this tension is applied.

sheet	\mathcal{A}	A (m ²)	m (kgm ⁻²)	B ($\times 10^{-6}$ Nm)	Re ($\times 10^5$)	T (N)	$\theta = 22.5^\circ$	$\theta = 45^\circ$
S2	1.33	0.7500	0.1410	59.65	0.59 - 5.18	2.06 - 7.95	✓	✓
S3	1.67	0.9375	0.1410	59.65	1.03 - 6.96	2.06 - 7.95	✓	✓
S4	2.00	1.1250	0.1410	59.65	1.01 - 8.17	2.06 - 7.95	✓	✓

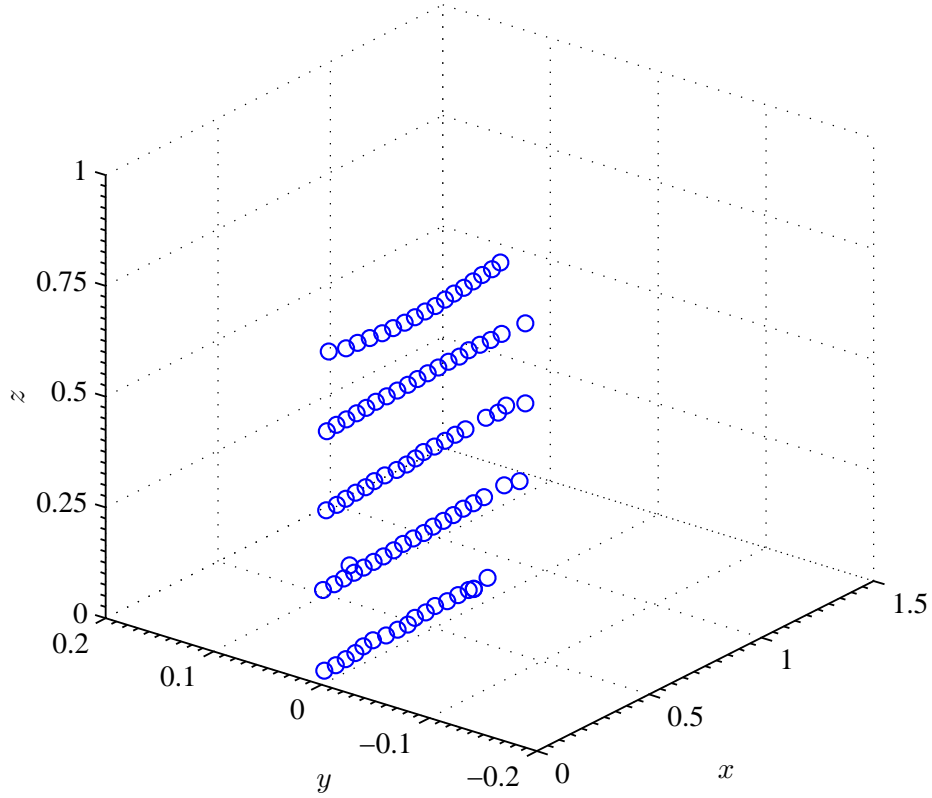


Figure 2: Markers positions on a perfectly stable sheet of length $L=1\text{m}$. These results correspond to an incident flow velocity of $U=2.37\text{ms}^{-1}$ with a combined tension of $T=7.95\text{N}$ applied at the trailing edge of the sheet.

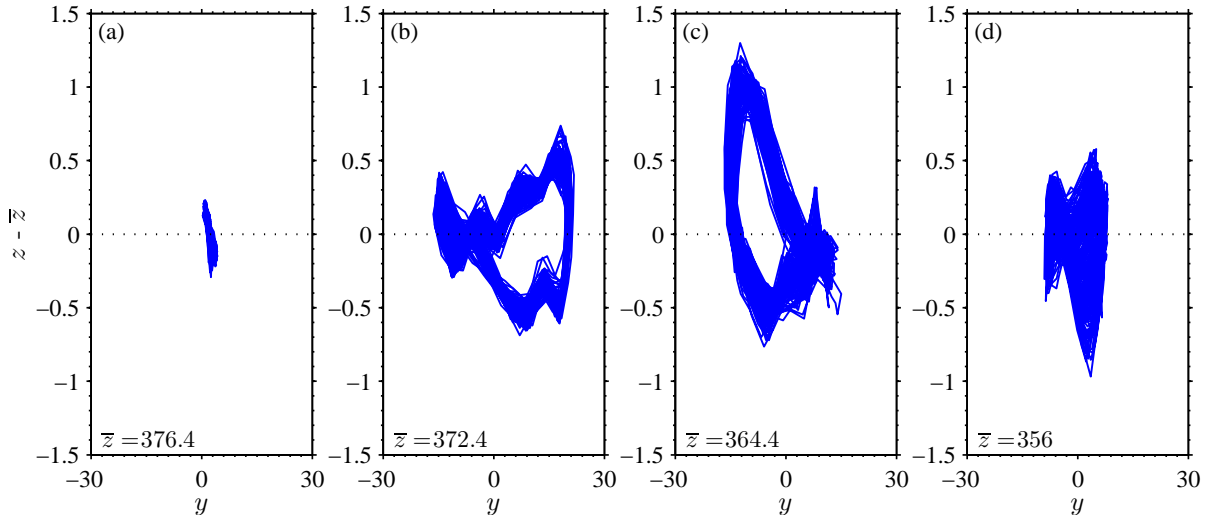


Figure 3: Trajectories of four markers in the (y,z) plane along the centre-line of a sheet. These results correspond to the same configuration pictured in Figure 2 with the fluid velocity increased to $U=7.26\text{ms}^{-1}$. The sheet is now unstable to flutter. The marker positions are: (a) $x\approx 0.05$; (b) $x\approx 0.35$; (c) $x\approx 0.70$; and (d) $x\approx 0.95$. The insert on the bottom left hand corner of each axis gives the mean vertical component of the displacement. All units are in $[\text{mm}]$.

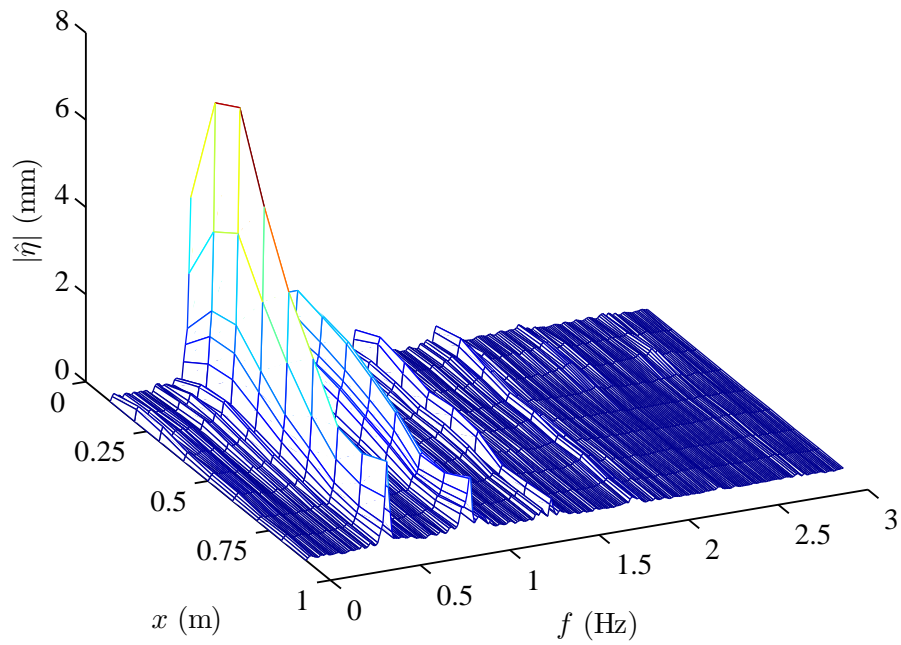


Figure 4: Spectral content of the displacement data for the markers along the centre-line of the sheet. The sheet is unstable at this incident flow velocity of $U=2.42\text{ms}^{-1}$. A combined tension of 2.06N is applied to the trailing edge in this example.

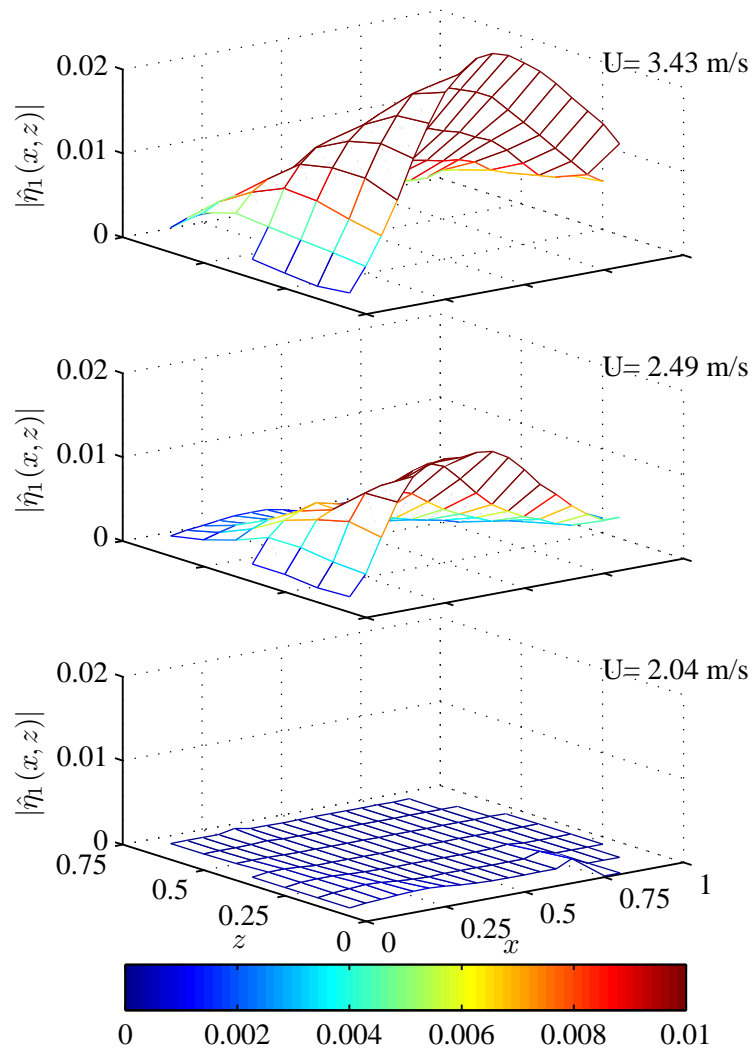


Figure 5: The magnitude of the first-harmonic component $|\eta(\omega_1)|$ of the sheet displacement. Its distributed is shown across the surface of the sheet located in the (x, z) plane. A combined tension of 2.06N is acting on the trailing edge. All units are in [m].

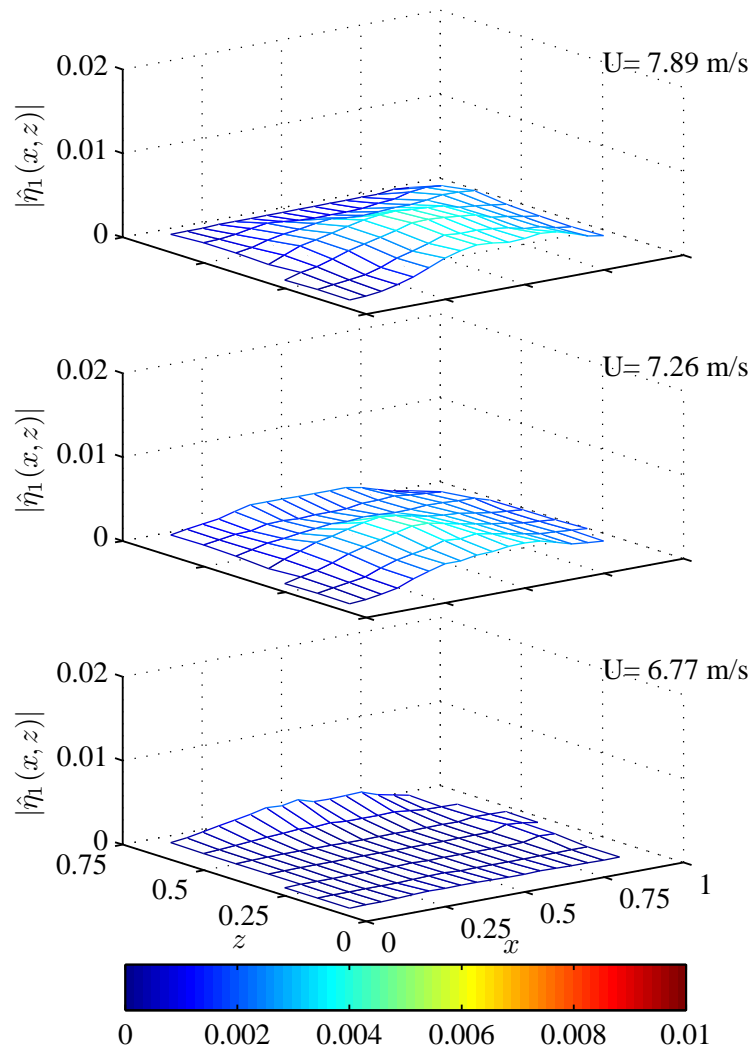


Figure 6: The magnitude of the first-harmonic component $|\eta(\omega_1)|$ of the sheet displacement. Its distributed is shown across the surface of the sheet located in the (x, z) plane. A combined tension of 5.98N is acting on the trailing edge. All units are in [m].

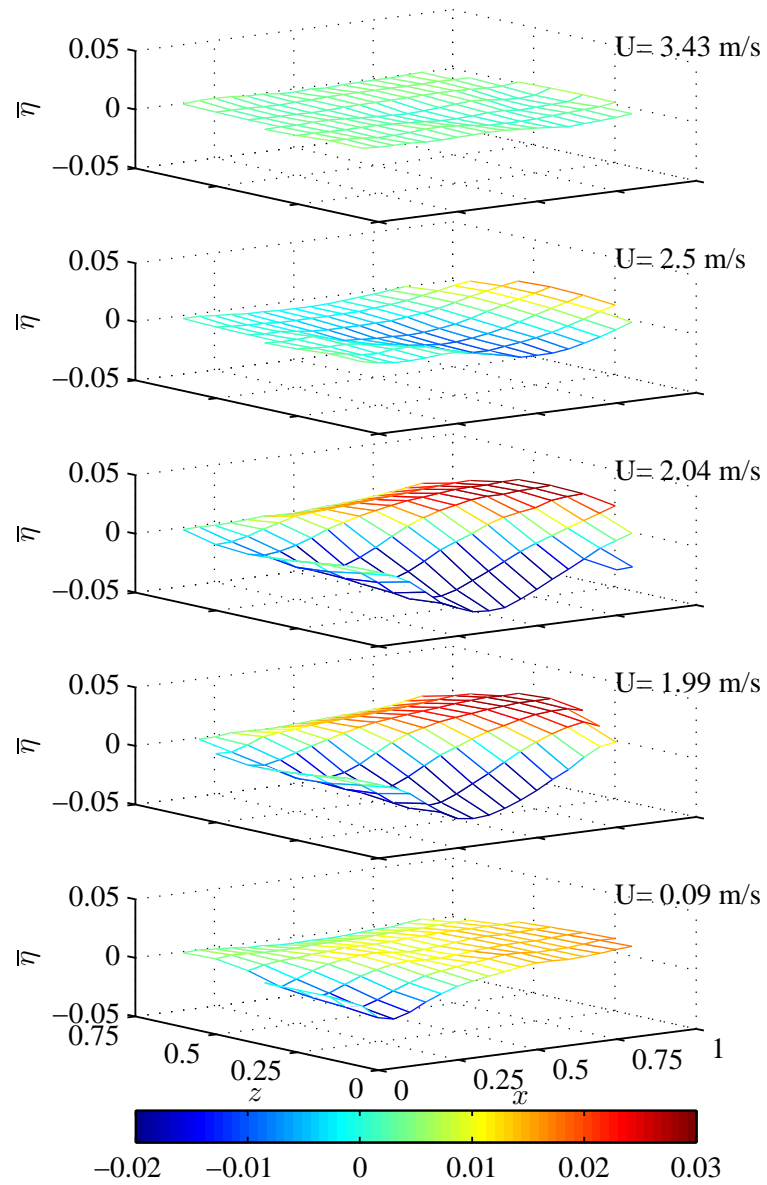


Figure 7: Magnitude of the zero-harmonic component across the surface of a sheet of length $L=1\text{m}$ and width $l=0.75\text{m}$ under a combined tension of $T=2.06\text{N}$.

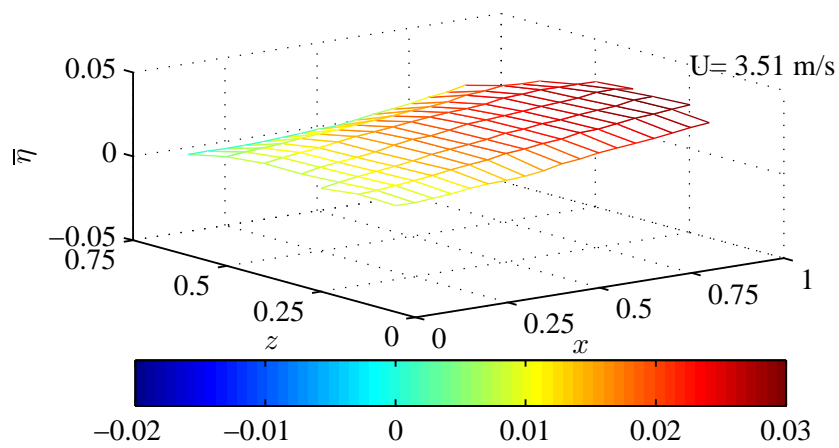


Figure 8: An example of the predominant mean component on the surface of a sheet. This particular example corresponds to a combined applied tension of $T=7.95\text{N}$ acting at $\theta=45^\circ$ to the trailing edge.